

High-Order Low Dissipation Conforming Finite-Element Discretization of the Maxwell Equations

Sébastien Jund¹, Stéphanie Salmon² and Eric Sonnendrücker^{1,*}

¹ IRMA, UMR 7501 Université de Strasbourg and CNRS, and CALVI project-team, INRIA Nancy Grand Est, 7 rue René Descartes, F-67084 STRASBOURG Cedex.

² Laboratoire de Mathématiques EA 4535, Université de Reims, U.F.R. Sciences Exactes et Naturelles, Moulin de la Housse - BP 1039, F-51687 REIMS cedex 2.

Received 10 March 2010; Accepted (in revised version) 23 May 2011

Communicated by Jan S. Hesthaven

Available online 28 October 2011

Abstract. In this paper, we study high order discretization methods for solving the Maxwell equations on hybrid triangle-quad meshes. We have developed high order finite edge element methods coupled with different high order time schemes and we compare results and efficiency for several schemes. We introduce in particular a class of simple high order low dissipation time schemes based on a modified Taylor expansion.

AMS subject classifications: 65M60

Key words: Maxwell's equations, edge finite element method, mass lumping, time discretization schemes.

1 Introduction

Our aim is to develop very precise and very efficient solvers for the Maxwell equations in time domain and in complex geometries. So, we will need high order methods for good precision and unstructured meshes to handle complex geometries.

The numerical solution of Maxwell's equations has been performed most reliably with the Finite Difference Time Domain Yee solver which has proved very robust, but comes to its limits when unstructured meshes need to be handled or when higher order is helpful. Hence, developing new efficient and reliable Maxwell solvers has been an area of intense research in the last 40 years. Different approaches have been followed to develop

*Corresponding author. *Email addresses:* stephanie.salmon@univ-reims.fr (S. Salmon), sonnen@math.unistra.fr (E. Sonnendrücker)

solvers that can handle unstructured meshes, the most important certainly being the Finite Element (FE) solvers including their discontinuous variants. Finite Element methods are better adapted for complex geometries as they can be based on different computational elements (hexahedra, tetrahedra) which can be used to mesh efficiently complex geometries. Finite Elements adapted to Maxwell's equations, the so-called edge elements have been introduced by Nédélec [29] in 1980. Moreover the Finite Element methodology gives easy access to higher order methods which have proved useful recently for several applications [3,33]. Let us also mention the concept of discrete differential forms (see [25] for a review) that provide new insights of the reasons why some solvers work well and other do not. One of the drawbacks of these edge finite element methods for Time Domain computations, is the need to solve a linear system at each time step, and therefore these methods are known to be expensive. For this reason mass-lumped elements for any order have been introduced on squares and cubes [7–9] and a quasi mass-lumped method has been proposed in [17]. Mass-lumped elements for first and second order edge elements have been developed on triangles [14] and tetrahedra [15]. Mass lumped nodal Finite Elements for a formulation of Maxwell's equations keeping the divergence constraint and adding a Lagrange multiplier have also been developed [1,5]. More recently a lot of effort has gone into the derivation of high-order Discontinuous Galerkin schemes [2,16,23,24,35] which completely eliminate the need for solving a global linear system. Apart from that let us also mention Finite Volume schemes which also can be made high order on unstructured grids [18]. A detailed review of high order methods by Hesthaven can also be found in [22].

Our aim in this paper is to study high-order conforming Finite Element schemes based on hybrid triangle-quad meshes for use in the time domain. In order to really keep high-order schemes, we will work not only with high-order schemes in space but also in time. We introduce in particular a very simple high-order time stepping scheme which is based on a stabilized (when needed) Taylor expansion method. Indeed after space discretization with our finite elements, we get a linear system of ordinary differential equations which conserves exactly a discrete energy and that can be written as $dU/dt = AU$ where A is a matrix with purely imaginary eigenvalues. An order p Taylor expansion scheme for this linear system reads $U^{n+1} = (I + \Delta t A + \dots + \frac{\Delta t^p}{p!} A^p) U^n$. Note that this scheme is equivalent to the unique p -stage, order p Runge-Kutta method for the linear system we consider [19,20]. Such a scheme is unstable for any Δt for some orders including 1, 2, 5 and 6, and stable for others including 3 and 4. Our stabilization method consists in adding an additional term ζA^{p+1} where ζ is chosen to stabilize the method, its order being conserved. Moreover ζ can also be tuned in order to get low dissipation. This yields stable arbitrary high order schemes which are very efficient, compared to existing schemes, for orders higher than 4. Note that the Strong Stability Preserving schemes advocated in [20] do apply only for space-discretized problems for which there is a negative real part of the eigenvalues for which explicit Euler is stable. This is the case for Discontinuous Galerkin methods with upwinding, but not for conforming Finite Elements like ours where the eigenvalues are purely imaginary. On the other hand, the modified equa-

tion approach can be used to get high order centered schemes [11] with optimized CFL. Unlike these works, the idea behind our method is to add some low dissipation effect in the high order time scheme in order to make long time or non linear simulation more robust.

The paper is organized as follows. First we recall the mixed variational formulation for the Maxwell equations and we construct our conforming families of finite elements spaces which satisfy an exact sequence property. We also verify that the edge element mass matrix can be lumped on uniform quads. Then we introduce our time discretization based on a stabilized Taylor expansion as well as high-order symplectic time-discretizations in order to compare their efficiency. Finally, we compare the efficiency of the different schemes for different grids and orders.

2 Variational formulation for the 2D Maxwell equations

2.1 The continuous problem

We consider the Maxwell equations in a subdomain $\Omega \subset \mathbb{R}^2$ supposed regular with a regular boundary denoted by $\Gamma = \partial\Omega$. We note \mathbf{n} , the outward unit normal vector of Ω on the boundary Γ . We recall that in 2D, we have two curl operators, one acting on scalars u , denoted by $\nabla \times u = (\frac{\partial u}{\partial y} \quad -\frac{\partial u}{\partial x})^T$, and one acting on vectors $\mathbf{v} = (v_x \quad v_y)^T$ denoted by $\nabla \times \mathbf{v} = \frac{\partial v_y}{\partial x} - \frac{\partial v_x}{\partial y}$. We also introduce the function spaces needed in the sequel

$$H(\text{curl}, \Omega) = \{ \mathbf{v} \in (L^2(\Omega))^2; \nabla \times \mathbf{v} \in L^2(\Omega) \}$$

and

$$H_0(\text{curl}, \Omega) = \{ \mathbf{v} \in H(\text{curl}, \Omega); \mathbf{v} \times \mathbf{n} = 0 \}.$$

Finally, we recall the Green formulas we will need

$$\int_{\Omega} (\nabla \times G) \cdot \mathbf{F} dX = \int_{\Omega} G(\nabla \times \mathbf{F}) dX - \int_{\Gamma} (G \times \mathbf{n}) \cdot \mathbf{F} dS, \forall \mathbf{F} \in H(\text{curl}, \Omega), \forall G \in H^1(\Omega), \quad (2.1)$$

and

$$\int_{\Omega} (\nabla \cdot \mathbf{F}) G dX = - \int_{\Omega} \mathbf{F} \cdot (\nabla G) dX + \int_{\Gamma} (\mathbf{F} \cdot \mathbf{n}) G dS, \forall \mathbf{F} \in H(\text{div}, \Omega), \forall G \in H^1(\Omega). \quad (2.2)$$

In bi-dimensional domains, Maxwell's equations can be decoupled into two systems. The first involving the (E_x, E_y, B_z) components is called the Transverse Electric (TE) mode, and the second, involving the (B_x, B_y, E_z) components is called the Transverse Magnetic (TM) mode. As both mode can be discretized in the same manner, we shall only consider

in the sequel the TE mode which reads

$$\frac{\partial \mathbf{E}}{\partial t} - \nabla \times B = -\mathbf{J}, \quad (2.3)$$

$$\frac{\partial B}{\partial t} + \nabla \times \mathbf{E} = 0, \quad (2.4)$$

$$\nabla \cdot \mathbf{E} = \rho, \quad (2.5)$$

where the components are defined by $\mathbf{E} = (E_x \ E_y)^T$, $B = B_z$. These equations need to be supplemented with initial and boundary conditions. We shall only consider perfectly conducting boundary conditions $\mathbf{E} \times \mathbf{n} = 0$.

Let us notice that Gauss' law (2.5) is a direct consequence of the continuity equation

$$\frac{\partial \rho}{\partial t} + \nabla \cdot \mathbf{J} = 0.$$

Indeed, taking formally the divergence of Ampere's law and replacing the divergence of \mathbf{J} by the time derivative of ρ implies the time derivative of Gauss' law. Hence assuming the latter is satisfied by the initial conditions, it remains satisfied for all times.

In order to derive a conforming Finite Element approximation of Maxwell's equations we first need to write an appropriate variational formulation. We would like to stay with the first order version of the system and are then naturally led to a mixed formulation involving two different functional spaces for \mathbf{E} and B . The two options are, after multiplying both equations by a test function and integrating by parts, to use a Green's formula for either one of the two equations but not for both.

Using the Green's formula (2.1) in Ampere's law (2.3) yields the variational formulation: Find $(\mathbf{E}, B) \in H_0(\text{curl}, \Omega) \times L^2(\Omega)$ such that

$$\frac{d}{dt} \int_{\Omega} \mathbf{E} \cdot \boldsymbol{\psi} \, dX - \int_{\Omega} B (\nabla \times \boldsymbol{\psi}) \, dX = - \int_{\Omega} \mathbf{J} \cdot \boldsymbol{\psi} \, dX, \quad \forall \boldsymbol{\psi} \in H_0(\text{curl}, \Omega), \quad (2.6)$$

$$\frac{d}{dt} \int_{\Omega} B \varphi \, dX + \int_{\Omega} (\nabla \times \mathbf{E}) \varphi \, dX = 0, \quad \forall \varphi \in L^2(\Omega). \quad (2.7)$$

As we have for $\phi \in H_0^1(\Omega)$ that $\nabla \phi \in H_0(\text{curl}, \Omega)$, we can use $\nabla \phi$ as a test function in the variational formulation of Ampere's law. Then using the continuity equation and the Green formula (2.2), it yields that

$$\frac{d}{dt} \int_{\Omega} \mathbf{E} \cdot \nabla \phi \, dX = \frac{d}{dt} \int_{\Omega} \rho \phi, \quad \forall \phi \in H_0^1(\Omega)$$

which is a weak form of the time derivative of Gauss' law (2.5). Hence we do not have to worry about it as it will automatically be satisfied in our framework, provided it is at $t=0$.

The other option we will not consider here, is to use the variational formulation obtained by applying the Green formula (2.1) on Faraday's law. The conclusion for the time scheme would be the same.

2.2 Discretization using conforming finite elements

In order to keep the specific features of Maxwell's equations at the discrete level which are useful in different contexts, we shall consider finite dimensional subspaces endowed with the same exact sequence structure as in the continuous level [25]. Let us first derive the linear system that comes out of this discretization. Let $\{\boldsymbol{\psi}_i\}_{i=1,\dots,N}$ be a basis of $W \subset H(\text{curl}, \Omega)$ and $\{\varphi_k\}_{k=1,\dots,M}$ a basis of $V \subset L^2(\Omega)$. Rewriting Eqs. (2.6) and (2.7) our goal is to solve the following problem: *Find $(\mathbf{E}, B) \in W \times V$ such that*

$$\begin{cases} \frac{d}{dt} \int_{\Omega} \mathbf{E} \cdot \boldsymbol{\psi}_i dX - \int_{\Omega} B(\nabla \times \boldsymbol{\psi}_i) dX = - \int_{\Omega} \mathbf{J} \cdot \boldsymbol{\psi}_i dX, & \forall i = 1, \dots, N, \\ \frac{d}{dt} \int_{\Omega} B \varphi_k dX + \int_{\Omega} (\nabla \times \mathbf{E}) \varphi_k dX = 0, & \forall k = 1, \dots, M, \end{cases} \quad (2.8)$$

which becomes when \mathbf{E} and B are decomposed on the respective bases of W and V

$$\begin{cases} M_w \dot{E} - KB = \tilde{J}, \\ M_v \dot{B} + K^T E = 0, \end{cases} \quad (2.9)$$

where E (resp. B) denote vectors of degrees of freedom and \dot{E} (resp. \dot{B}) is the time derivative of those vectors, with

$$\begin{aligned} (M_w)_{1 \leq i, j \leq N} &= \int_{\Omega} \boldsymbol{\psi}_j \cdot \boldsymbol{\psi}_i dX, \quad (M_v)_{1 \leq i, j \leq M} = \int_{\Omega} \varphi_i \varphi_j dX, \\ (K)_{1 \leq i \leq N, 1 \leq j \leq M} &= \int_{\Omega} \varphi_j (\nabla \times \boldsymbol{\psi}_i) dX. \end{aligned}$$

In the variational formulation of Faraday's law, (i.e. in the second equation of system (2.8)), $\nabla \times \mathbf{E} \in V$ because of the structure of our discrete spaces. Hence we can express $\nabla \times \mathbf{E}$ on the basis $\{\varphi_k\}_{k=1,\dots,M}$ of V which yields

$$\nabla \times \mathbf{E} = \sum_{l=1}^M \sigma_l^V (\nabla \times \mathbf{E}) \varphi_l = \sum_{l=1}^M \sigma_l^V \left(\sum_{j=1}^N \sigma_j^W (\mathbf{E}) (\nabla \times \boldsymbol{\psi}_j) \right) \varphi_l = \sum_{l=1}^M \sum_{j=1}^N \sigma_j^W (\mathbf{E}) \sigma_l^V (\nabla \times \boldsymbol{\psi}_j) \varphi_l.$$

In particular we get that $\sigma_l^V (\nabla \times \mathbf{E}) = \sum_{j=1}^N \sigma_j^W (\mathbf{E}) \sigma_l^V (\nabla \times \boldsymbol{\psi}_j)$, and injecting this expression in the discrete Faraday law

$$\int_{\Omega} (\nabla \times \mathbf{E}) \varphi_k dX = \sum_{l=1}^M \sum_{j=1}^N \int_{\Omega} \varphi_l \varphi_k dX \sigma_l^V (\nabla \times \boldsymbol{\psi}_j) \sigma_j^W (\mathbf{E}),$$

which is the k^{th} line (for k from 1 to M) of the vector $M_v R E$ where R is the matrix defined by

$$(R)_{1 \leq i \leq M, 1 \leq j \leq N} = \sigma_i^V (\nabla \times \boldsymbol{\psi}_j),$$

so that the system (2.9) can be written equivalently in the form

$$\begin{cases} M_w \dot{E} - KB = \tilde{J}, \\ \dot{B} + RE = 0. \end{cases} \quad (2.10)$$

This new formulation yields an explicit expression of B which can then be computed without solving a linear system.

On rectangular meshes, the actual subspaces $W \subset H(\text{curl}, \Omega)$ and $V \subset L^2(\Omega)$ are defined as follows

$$\begin{aligned} W &= \left\{ \boldsymbol{\psi} \in H(\text{curl}, \Omega) \mid \boldsymbol{\psi}|_{K_i} \in \begin{pmatrix} \mathbf{Q}_{k-1,k}(K_i) \\ \mathbf{Q}_{k,k-1}(K_i) \end{pmatrix}, \forall i=1, \dots, r \right\}, \\ V &= \{ \varphi \in L^2(\Omega) \mid \varphi|_{K_i} \in \mathbf{Q}_{k-1}(K_i), \forall i=1, \dots, r \}, \end{aligned}$$

where

$$\mathbf{Q}_{m,n} = \langle x^i y^j \mid 0 \leq i \leq m, 0 \leq j \leq n \rangle.$$

The space W is known as the first family of edge elements $H(\text{curl})$ -conforming of Nédélec [29] and the space V is the space of discontinuous functions which restrict to a polynomial of degree $k-1$ with respect to each variable on each cell. This is the kind of approximation used in Discontinuous Galerkin methods.

On triangular cells the discrete spaces are defined by

$$\begin{aligned} W &= \left\{ \boldsymbol{\psi} \in H(\text{curl}, \Omega) \mid \boldsymbol{\psi}|_{T_i} \in \mathbb{P}_{k-1}^2(T_i) + \overline{\mathbb{P}}_{k-1}(T_i) \begin{pmatrix} y \\ -x \end{pmatrix}, \forall i=1, \dots, r \right\}, \\ V &= \{ \varphi \in L^2(\Omega) \mid \varphi|_{T_i} \in \mathbb{P}_{k-1}(T_i), \forall i=1, \dots, r \}, \end{aligned}$$

where $\overline{\mathbb{P}}_{k-1}$ denotes the set of polynomials of degree exactly $k-1$. The space V is \mathbb{P}_{k-1} on each element and discontinuous across element boundaries (conforming in $L^2(\Omega)$), so is straightforward to construct. For the space W , we have again used the first family of edge elements of Nédélec [29], conforming in $H(\text{curl}, \Omega)$, but we have changed the degrees of freedom.

Remark 2.1. Conformal coupling of edge elements on triangles and quads. Uniform Cartesian meshes with identical square cells and triangular meshes have both advantages and drawbacks. On the one hand, the data structure needed to implement Cartesian meshes is much lighter and one can take advantage of its specific form to accelerate computations. On the other hand they cannot easily handle complex geometries. Therefore a natural idea is to use hybrid meshes made of uniform square cells in the largest possible zone and of triangles close to the boundaries. An example of such a mesh is given in Fig. 1. First, we want to make sure that the approximation space based on our edge finite elements on both quads and triangles is still included in $H(\text{curl}, \Omega)$. Second, we want to ensure that the sequence of discrete spaces on this mesh is still an exact one. This can be verified easily as we have chosen the degrees of freedom in such a way that they correspond on edges shared by quads and triangles.

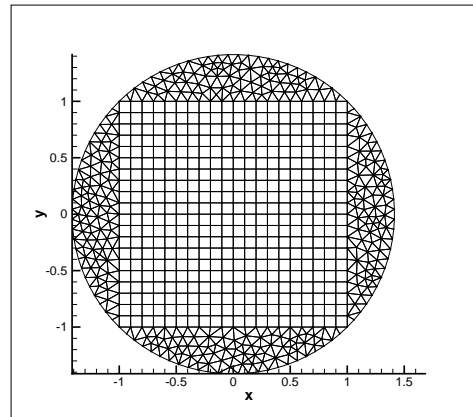


Figure 1: Example of hybrid mesh of a disk.

3 Lumping of mass matrix

When solving the Maxwell equations with Finite Elements in the time domain, a linear system involving the mass matrix needs to be solved at each time step, which can be very costly. This is one of the reasons of the popularity of Discontinuous Galerkin methods [23] for which the mass matrix is always at least block diagonal with fairly small blocks so that the linear system can be solved very quickly. Concerning continuous Finite Element methods for wave propagation in the time domain, a lot of effort has been made to construct new Lagrange Finite Elements using approximate mass matrices that are diagonal without impairing the order of the method [6]. There have been efforts in this direction as well for Edge elements. In particular for the triangles of lowest order, a mass lumping scheme has been proposed by Haugazeau and Lacoste [27]. On the other hand, on a rectangular quadrilateral mesh, there is a natural way to perform the mass lumping as pointed out by Cohen and Monk [9]. Other mass lumping schemes for the Maxwell equations have been proposed by Elm kies and Joly [14] for triangular elements and by Cohen and co-authors [6, 30] for arbitrary quadrilateral meshes but they add degrees of freedom on the edges which are not tangential and therefore are difficult to put into an exact sequence framework. Therefore we shall not consider mass lumping on triangles.

On rectangles, we can choose basis functions which are products of Legendre and Lagrange polynomials in one variable and thus naturally lead to mass lumping. Indeed, by choosing the Gauss-Lobatto points as degrees of freedom associated to the Lagrange polynomials $L_{\tilde{\zeta}_i}$ (where $\tilde{\zeta}_i$ is equal to x_i or y_i) and using the associated high-order Gauss quadrature formula we get

$$\int_K \psi_{\tilde{\zeta}_i}^m \cdot \psi_{\tilde{\zeta}_j}^n dX = \delta_{\tilde{\zeta}_i \tilde{\zeta}_j} \delta_{mn} \int_0^1 L_{\tilde{\zeta}_i}(\tilde{\zeta}) L_{\tilde{\zeta}_j}(\tilde{\zeta}) d\tilde{\zeta} \simeq \omega_i \delta_{ij} \delta_{\tilde{\zeta}_i \tilde{\zeta}_j} \delta_{mn}, \quad \forall \psi_{\tilde{\zeta}_i}^m, \psi_{\tilde{\zeta}_j}^n \in W,$$

where $\{\omega_i\}_{i=0, \dots, k}$ are the weights associated to the quadrature formula.

4 Time discretization

As for wave propagation problems, due to the CFL condition, explicit schemes generally use a time step of the same order as the typical cell size in the space discretization. Then, it is desirable to have a time stepping scheme which is of the same order as the space discretization one. Typical time stepping schemes that can be used up to an arbitrary order for equations of the same form as ours are Runge-Kutta schemes [19,23], symplectic schemes [4, 31, 32, 38], modified equation schemes [10, 34], or Cauchy-Kovalewski type techniques [12,13,21].

4.1 A Taylor expansion method

After our Finite Element space discretization, we get a system of linear ordinary differential equations of the form

$$\frac{dU}{dt} = AU, \quad (4.1)$$

where U is the time-dependent unknown vector and A a constant coefficient matrix. For such a system, where the time derivatives can easily be computed using Eq. (4.1), $\frac{d^k U}{dt^k} = A^k U$, the simplest way to get an order p method is to use a Taylor expansion of U between t_n and t_{n+1} , where $t_n = n\Delta t$, for a time step Δt :

$$U(t_{n+1}) = U(t_n) + \Delta t \frac{dU(t_n)}{dt} + \frac{\Delta t^2}{2!} \frac{d^2 U(t_n)}{dt^2} + \dots + \frac{\Delta t^p}{p!} \frac{d^p U(t_n)}{dt^p} + \mathcal{O}(\Delta t^{p+1}).$$

Then replacing the time derivatives by powers of A we get

$$U(t_{n+1}) = U(t_n) + \Delta t A U(t_n) + \frac{\Delta t^2}{2!} A^2 U(t_n) + \dots + \frac{\Delta t^p}{p!} A^p U(t_n) + \mathcal{O}(\Delta t^{p+1}).$$

Note that if we interpret the matrix vector multiplication AU as a discrete space derivative, this method can be assimilated to the Cauchy-Kovalewski technique advocated by [12,13].

Following this idea, the successive approximations U_n of $U(t_n)$ are given by the scheme:

$$U_{n+1} = \left(I + \Delta t A + \frac{\Delta t^2}{2!} A^2 + \dots + \frac{\Delta t^p}{p!} A^p \right) U_n. \quad (4.2)$$

We now denote by \mathbb{A} the amplification matrix

$$\mathbb{A} = I + \Delta t A + \frac{\Delta t^2}{2!} A^2 + \dots + \frac{\Delta t^p}{p!} A^p.$$

The numerical time stepping scheme then reduces to $U_{n+1} = \mathbb{A}U_n$ and will be stable provided $\|\mathbb{A}\| \leq 1$.

It is well known that for any matrix \mathbb{A} ,

$$\rho(\mathbb{A}) \leq \|\mathbb{A}\|,$$

where $\rho(\mathbb{A})$ is the spectral radius of \mathbb{A} , *i.e.* the largest modulus of an eigenvalue of \mathbb{A} . Moreover both quantities are equal when the matrix \mathbb{A} is symmetric or skew symmetric.

Let us now assume that the starting matrix A is symmetric (resp. skew-symmetric), A is then diagonalizable and all its eigenvalues are real (resp. imaginary). Then, given an eigenvalue λ of A , it is easy to see that $1 + \Delta t \lambda + \dots + \frac{\Delta t^p}{p!} \lambda$ is an eigenvalue of \mathbb{A} (and that all the eigenvalues of \mathbb{A} can be expressed in a similar way from the eigenvalues of A). In order to study the stability of the time discretization it is thus enough to find the zone of the complex plane where the polynomial function of one complex variable $\mu = \Delta t \lambda$ given by $R(\mu) = 1 + \mu + \dots + \frac{\mu^p}{p!}$, is of modulus less than 1.

Using MAPLE[©] we plot the stability regions in Fig. 2.

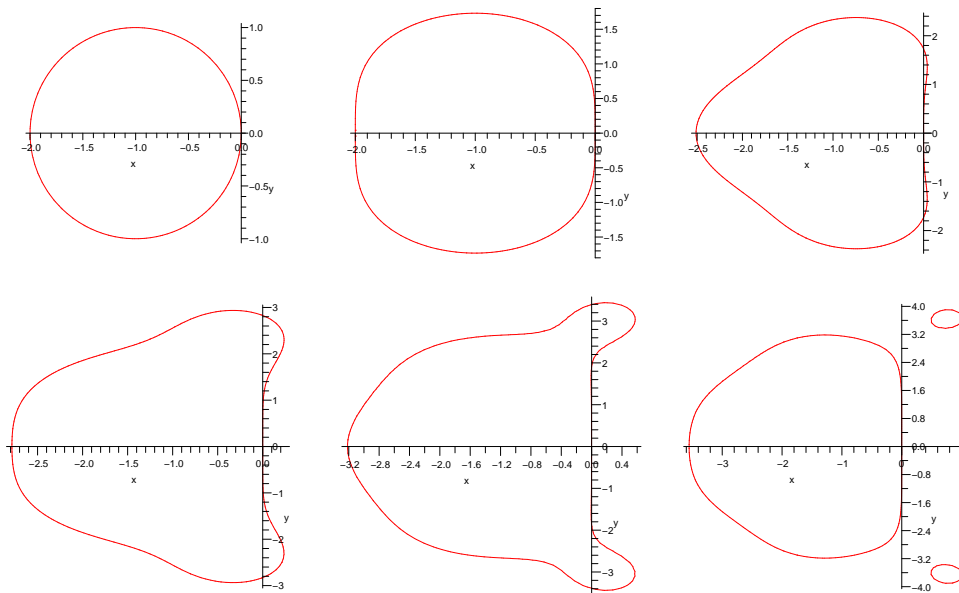


Figure 2: Stability regions for the time discretizations of order 1 to 6 (from left to right and top to bottom).

4.1.1 Application to Maxwell's equations

Let us recall the space-discretized Maxwell equations we obtained

$$M_w \frac{dE}{dt} - KB = 0, \tag{4.3}$$

$$M_v \frac{dB}{dt} + K^T E = 0, \tag{4.4}$$

that we can rewrite as

$$\frac{d}{dt} \begin{pmatrix} E \\ B \end{pmatrix} = \underbrace{\begin{pmatrix} 0 & M_w^{-1}K \\ -M_v^{-1}K^T & 0 \end{pmatrix}}_A \begin{pmatrix} E \\ B \end{pmatrix}.$$

Proposition 4.1. *If λ denotes a non vanishing eigenvalue of A associated to the eigenvector $(E \ B)^T$, then $-\lambda^2$ is an eigenvalue of $M_v^{-1}K^T M_w^{-1}K$ and $M_w^{-1}K M_v^{-1}K^T$ associated respectively to the eigenvectors B and E , and λ is purely imaginary.*

Conversely if μ denotes a non vanishing eigenvalue of $M_v^{-1}K^T M_w^{-1}K$, then μ is also eigenvalue of $M_w^{-1}K M_v^{-1}K^T$ and, μ is real and strictly positive and $\lambda = \pm i\sqrt{\mu}$ is an eigenvalue of A .

Proof. Let $\lambda \neq 0$ be a non vanishing eigenvalue of A associated to the eigenvector $(E \ B)^T$, then we have:

$$M_w^{-1}KB = \lambda E, \quad (4.5)$$

$$-M_v^{-1}K^TE = \lambda B. \quad (4.6)$$

Note that necessarily E and B are non zero: assume $E = 0$ then by (4.5), λB is vanishing which implies $B = 0$, as λ is non zero. In a same way, if $B = 0$, we can prove that E is vanishing also.

By multiplying (4.5) by $M_v^{-1}K^T$ and using (4.6), we obtain

$$M_v^{-1}K^T M_w^{-1}KB = \lambda M_v^{-1}K^TE = -\lambda^2 B.$$

Then $-\lambda^2$ is an eigenvalue of $M_v^{-1}K^T M_w^{-1}K$ associated to the eigenvector B . Similarly, we have

$$M_w^{-1}K M_v^{-1}K^TE = -\lambda M_w^{-1}KB = -\lambda^2 E,$$

then $-\lambda^2$ is an eigenvalue of $M_w^{-1}K M_v^{-1}K^T$ associated to the eigenvector E . If we consider $\mu \neq 0$ eigenvalue of $M_v^{-1}K^T M_w^{-1}K$ associated to the eigenvector B . Then,

$$K^T M_w^{-1}KB = \mu M_v B,$$

and multiplying by \bar{B}^T , we obtain

$$(\bar{K}B)^T M_w^{-1}KB = \mu \bar{B}^T M_v B.$$

As matrices M_w^{-1} and M_v are symmetric and positive definite, $\mu \geq 0$. Then $-\lambda^2$ is positive which implies that λ is purely imaginary. Same result by considering the eigenvalues of $M_w^{-1}K M_v^{-1}K^T$.

Conversely, consider $\mu \neq 0$ eigenvalue of $M_v^{-1}K^T M_w^{-1}K$ associated to the eigenvector B , then we have:

$$M_v^{-1}K^T M_w^{-1}KB = \mu B.$$

Letting

$$E = \pm \frac{1}{i\sqrt{\mu}} M_w^{-1} K B = \mp \frac{i}{\sqrt{\mu}} M_w^{-1} K B,$$

E is non vanishing (μ and B are non vanishing), and the equation can be rewritten

$$\pm i\sqrt{\mu} M_v^{-1} K^T E = \mu B,$$

or

$$M_v^{-1} K^T E = \mp i\sqrt{\mu} B.$$

Then $M_w^{-1} K B = \pm i\sqrt{\mu} E$, and $-M_v^{-1} K^T E = \pm i\sqrt{\mu} B$, which means that $\pm i\sqrt{\mu}$ is an eigenvalue of A . We deduce

$$\begin{aligned} M_v^{-1} K^T E &= (\pm) 2\mu K^{-1} M_w E, \\ M_w^{-1} K M_v^{-1} K^T E &= \mu E. \end{aligned}$$

Finally μ is also an eigenvalue of $M_w^{-1} K M_v^{-1} K^T$. \square

Remark 4.1. This proposition tells us first that for the matrix A issued from the space discretization of Maxwell's equations, the eigenvalues are pure imaginary; and second, as the spectral radius of

$$A = \begin{pmatrix} 0 & M_w^{-1} K \\ -M_v^{-1} K^T & 0 \end{pmatrix}$$

is the same as the spectral radius of $M_w^{-1} K M_v^{-1} K^T$ or of $M_v^{-1} K^T M_w^{-1} K$, that the stability condition for the second order wave formulation and for the first order system are equivalent.

4.1.2 Stabilization of the time discretization

Actually, as we can see in Fig. 2, the discretizations of order 1, 2, 5 and 6 are unstable for any $\Delta t > 0$ for systems which have their eigenvalues on the imaginary axis, as in our case. Indeed these all have a neighborhood in the vicinity of zero where the imaginary axis is not included in the stability zone. Note in particular that the order 1 discretization corresponds to the forward Euler time scheme which is unstable in our case. Hence the SSP p -stage, p^{th} order Runge-Kutta methods which are equivalent to our formulation for the linear case [19] cannot claim anything about stability. Note that these methods were originally designed for dissipative space discretizations (upwind) for which the forward Euler method is stable for small enough Δt as the eigenvalues all strictly lie on the left half of the imaginary axis.

Our aim is now to stabilize the Taylor expansion methods for problems involving only eigenvalues on the imaginary axis without changing the order. This can be done for a method of order p by adding a term of the form ζA^{p+1} to \mathbb{A} . More precisely, we are looking for ζ such that the intersection of the imaginary axis with the stability zone

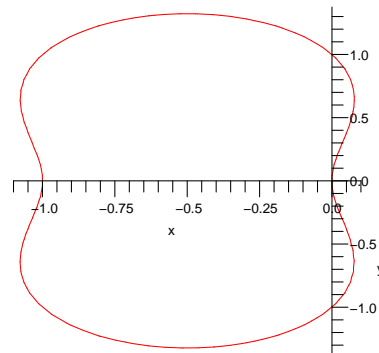


Figure 3: Stabilization of the order 1 time discretization.

contains a non empty interval as large as possible around 0. For example, for the first order method our stability region will consist of the μ such that

$$R(\mu) = 1 + \mu + \zeta \frac{\mu^2}{2!}$$

is of modulus less than 1. By taking $\mu = iy$ with $y \in \mathbb{R}$, we get that $|R(iy)| = 1$ for $y = 0$ or for $y^2 = 4(\zeta - 1)/\zeta^2$. By computing its derivative with respect to ζ we see that this last term is maximized for $\zeta = 2$, in which case $y^2 = 1$. So that the stability interval on the imaginary axis is $[-i, i]$ and the stability condition for our linear system of ordinary differential equations is $\Delta t \rho(A) \leq 1$. Fig. 3 represents the stability region for $\zeta = 2$.

For the order 2 discretization, we get the modified stability polynomial

$$R(\mu) = 1 + \mu + \frac{\mu^2}{2!} + \zeta \frac{\mu^3}{3!}.$$

The same procedure as for the first order yields that $|R(iy)| = 1$ for $y = 0$ or for $y^2 = (12\zeta - 9)/\zeta^2$ which is maximized for $\zeta = \frac{3}{2}$. The stability interval on the imaginary axis is then $[-2i, 2i]$ (see Fig. 4) and the stability constraint becomes $\Delta t \rho(A) \leq 2$.

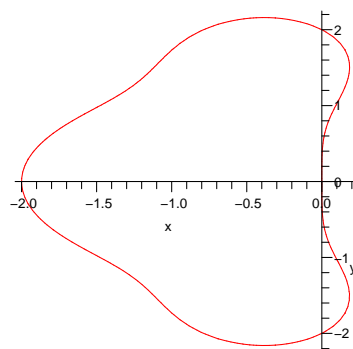


Figure 4: Stabilization of the order 2 time discretization.

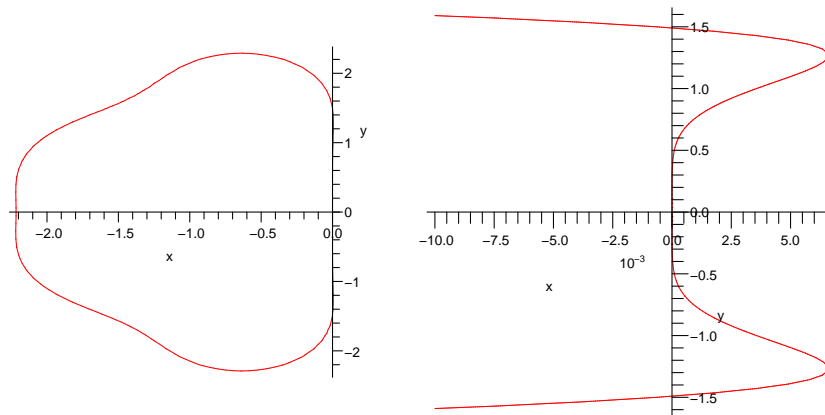


Figure 5: Stabilization of the order 5 time discretization: zoom around the imaginary axis.

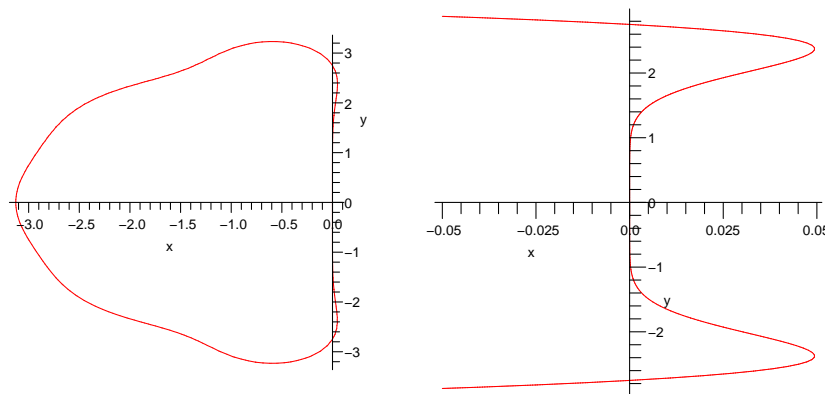


Figure 6: Stabilization of the order 6 time discretization: zoom around the imaginary axis.

For the order 5 discretization, we get the modified stability polynomial

$$R(\mu) = 1 + \mu + \frac{\mu^2}{2!} + \frac{\mu^3}{3!} + \frac{\mu^4}{4!} + \frac{\mu^5}{5!} + \zeta \frac{\mu^6}{6!}.$$

In this case we determine the optimal value of ζ numerically by a dichotomy algorithm and we get $\zeta \simeq 6.15746160$. The stability interval is then $[-1.491320186i, 1.491320186i]$ (Fig. 5) and the stability constraint becomes $\Delta t \rho(A) \leq 1.491320186$.

We conclude with the stabilization of the order 6 discretization for which the modified stability polynomial is

$$R(\mu) = 1 + \mu + \frac{\mu^2}{2!} + \frac{\mu^3}{3!} + \frac{\mu^4}{4!} + \frac{\mu^5}{5!} + \frac{\mu^6}{6!} + \zeta \frac{\mu^7}{7!}.$$

Numerically we get the optimal value $\zeta \simeq 2.505288240$, the stability interval then being $[-2.751711543i, 2.751711543i]$ (Fig. 6) and the stability constraint $\Delta t \rho(A) \leq 2.751711543$.

4.1.3 Low dissipation time discretization

As recognized by Hu et al. in [26], Runge-Kutta solvers like RK3 and RK4 can suffer from high dissipation when the maximal stability time step is used. This problem needs also be addressed with our stabilized Taylor expansion method, although the behavior is different as we shall see. Let us now look more closely at this dissipation problem in order to be able to choose a time step yielding lower dissipation and thus more cost-effective for the same accuracy in spite of a smaller time-step. This analysis will also be performed for the stable order 3 and 4 solvers in order to pinpoint the differences. Let us now proceed order by order to analyze the stability and dissipativity properties of the scheme.

For $\mu = iy$ on the imaginary axis, we define for a stabilized order p method

$$T_{\xi}(y) = |R(\mu)|^2 = \left| 1 + iy + \frac{(iy)^2}{2} + \dots + \frac{(iy)^p}{p!} + \xi \frac{(iy)^{p+1}}{(p+1)!} \right|^2.$$

The method is stable, if there exists $\tau > 0$ such that $T_{\xi}(y) \leq 1$ for $|y| < \tau$. Moreover, in order to minimize dissipativity we want to have $T_{\xi}(y)$ as close as possible to 1 for $|y| < \tau$. Introducing $D_{\xi}(y) = 1 - T_{\xi}(y)$ our problems amount to finding a stability zone defined by $\tau > 0$ such that $D_{\xi}(y) \geq 0$ for $|y| < \tau$. Moreover the amount of dissipation will be characterized by $\sigma(\xi) = \max_{|y| < \tau} D_{\xi}(y)$. In some cases, as for RK3 and RK4, it is useful to take τ less than the maximal stability zone in order to minimize dissipativity.

Order 1. In this case

$$D_{\xi}(y) = 1 - T_{\xi}(y) = 1 - \left| 1 + iy + \xi \frac{(iy)^2}{2} \right|^2 = y^2 \left((\xi - 1) - \xi^2 \frac{y^2}{4} \right).$$

The method is stable if $D_{\xi}(y) \geq 0$ in some neighborhood of 0, which is the case if $\xi > 1$, in this case $D_{\xi}(y) \geq 0$ for $|y| < \tau_{\xi} = \frac{2}{\xi} \sqrt{\xi - 1}$. The maximal stability zone is recovered by maximizing τ_{ξ} for $\xi > 1$. We then find that the maximal value of τ_{ξ} is one and is attained for $\xi = 2$. This gives us the maximal stability zone that we already computed in the previous subsection.

Now for a given value of ξ such that there exists a non empty stability zone, the dissipation is measured by $\sigma(\xi) = \max_{|y| < \tau_{\xi}} D_{\xi}(y)$. This value can be easily computed here and is $\sigma(\xi) = (\xi - 1) / \xi^2$.

In Fig. 7, we see on the left picture that the amount of dissipation can be reduced a lot when going from the maximal stability zone of $\xi = 2$ to $\xi = 1.1$ whereas the maximum time step is less than a factor of two between these two values of ξ . The amount of dissipation is plotted on the right picture. It is highest (0.13397) for the maximal stability zone. Depending on the amount of dissipation one wants, or one can afford, it is possible to choose an appropriate value of ξ between 1 and 2.

Order 2. We now get $T_{\xi}(y) = (1 - \frac{y^2}{2})^2 + (y - \xi \frac{y^3}{6})^2$, so that

$$D_{\xi}(y) = 1 - T_{\xi}(y) = \frac{y^4}{36} (12\xi - 9 - \xi^2 y^2).$$

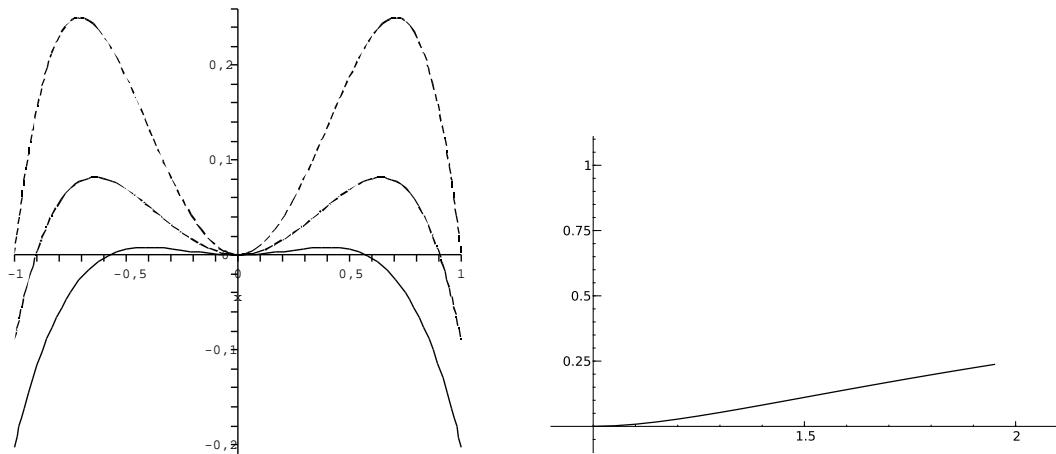


Figure 7: Order 1. Left. Plots of $D_\zeta(y)$ for $\zeta = 1.1$ (solid), $\zeta = 1.4$ (dotted), $\zeta = 2$ (dashed). Right. Maximum dissipation for different values of ζ going for 1 (minimal stability zone) to 2 (maximal stability zone).

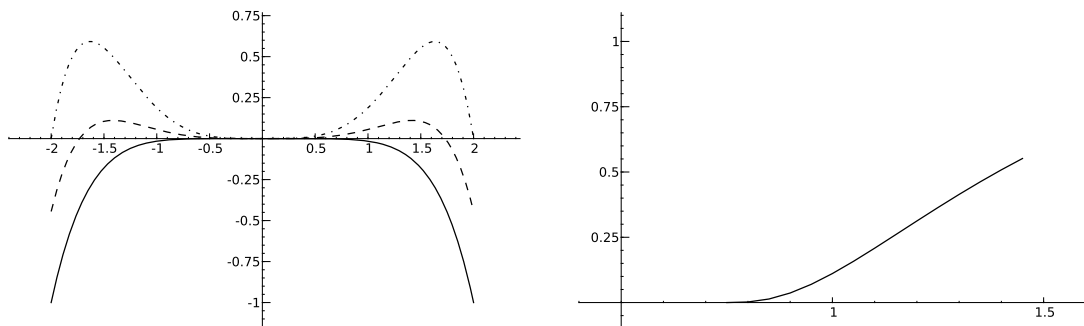


Figure 8: Order 2. Left. Plots of $D_\zeta(y)$ for $\zeta = 0.75$ (solid), $\zeta = 1.0$ (dash), $\zeta = 1.5$ (dash-dot). Right. Maximum dissipation for different values of ζ going for 0.75 (minimal stability zone) to 1.5 (maximal stability zone).

Hence $D_\zeta(y) \geq 0$ in the neighborhood of 0 provided $\zeta > 3/4$, in which case the stability zone is $|y| < \tau_\zeta = \sqrt{12\zeta - 9}/\zeta$. The maximal stability zone is reached for $\zeta = 3/2$ and the corresponding $\tau_\zeta = 2$. The maximal dissipation is here $\sigma(\zeta) = (4\zeta - 3)^3 / (9\zeta^4)$. For $\zeta = 0.78$, we have $\tau_\zeta \approx 0.75$ and $\sigma(\zeta) < 0.001$. For $\zeta = 0.96$, we have $\tau_\zeta \approx 0.96$ and $\sigma(\zeta) < 0.0023$. For $\zeta = 1.5$, we have $\tau_\zeta = 2$ and $\sigma(\zeta) \approx 0.6$. See Fig. 8.

Order 3. We now get

$$D_\zeta(y) = 1 - T_\zeta(y) = 1 - \left| 1 + iy + \frac{(iy)^2}{2} + \frac{(iy)^3}{3!} + \zeta \frac{(iy)^4}{4!} \right|^2$$

$$= \frac{y^4}{24} \left((1 - \zeta) + \left(\frac{\zeta}{2} - \frac{1}{3} \right) y^2 - \frac{\zeta^2}{48} y^4 \right).$$

Hence $D_\zeta(y) \geq 0$ in the neighborhood of 0 provided $\zeta \leq 1$. The maximal stability zone is

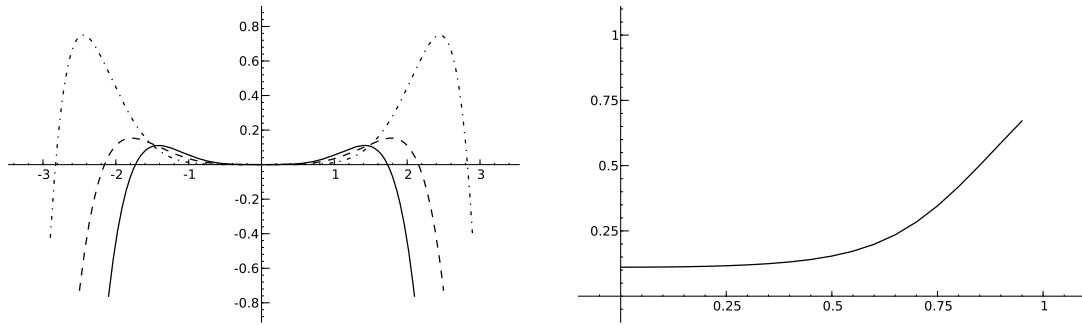


Figure 9: Order 3. Left. Plots of $D_\zeta(y)$ for $\zeta=0$ (dash dot), $\zeta=0.5$ (dash), $\zeta=1$ (solid). Right. Maximum dissipation for different values of ζ going for 0 (minimal stability zone) to 1 (maximal stability zone).

obtained for $\zeta_0=1$ and $\tau_{\zeta_0}=2\sqrt{2}$. Note that for $\zeta=1$, the scheme is exactly our fourth order scheme. In this case Fig. 9 shows that the dissipation is larger than 0.1 for any value of $\zeta \in [0,1]$. Moreover, we see on the left hand side of the figure, that the dissipation is lowest close to 0 for larger values of ζ . Hence the best option in this case to reduce dissipation is to take $\zeta=1$, but not to go to the maximal stability condition, but use a smaller time step. For $\zeta=1$, $D_\zeta(y) \sim y^6/72$ in the neighborhood of 0. Hence it goes quickly to 0 for fairly large values of y . For example $D_1(0.75) \approx 2.3 \times 10^{-2}$, $D_1(0.5) \approx 2.1 \times 10^{-3}$.

Order 4. We have

$$D_\zeta(y) = 1 - T_\zeta(y) = 1 - \left| 1 + iy + \frac{(iy)^2}{2} + \frac{(iy)^3}{3!} + \frac{(iy)^4}{4!} + \zeta \frac{(iy)^5}{5!} \right|^2$$

$$= y^6 \left(\frac{1}{72} - \frac{\zeta}{60} + \left(\frac{\zeta}{360} - \frac{1}{24^2} \right) y^2 - \frac{\zeta^2}{120^2} y^4 \right).$$

The dominating term close to 0 in the expression is $y^6(1/72 - \zeta/60)$. This is positive provided $\zeta \leq 5/6$ so that $D_\zeta(y) \geq 0$ in the neighborhood of 0 provided $\zeta \leq 5/6$, which yields a non vanishing stability zone. The maximal stability zone is obtained for $\zeta_0=5/6$ and by dichotomy we get that $\tau_{\zeta_0} \approx 3.46$. The situation here is the same as for order 3. The dissipation does not go to 0 for small ζ (see Fig. 10). The smallest dissipation around 0 is given for $\zeta=5/6$, in which case $D_\zeta(y) \sim Cy^8$ in the neighborhood of 0, where C is a positive constant. So by taking y small enough, we can get very small dissipation. For example $D_{5/6}(1.5) = 0.012$, $D_{5/6}(1) = 0.00053$, $D_{5/6}(0.5) = 5.5 \times 10^{-5}$.

Order 5. We have

$$D_\zeta(y) = 1 - T_\zeta(y) = 1 - \left| 1 + iy + \frac{(iy)^2}{2} + \frac{(iy)^3}{3!} + \frac{(iy)^4}{4!} + \frac{(iy)^5}{5!} + \zeta \frac{(iy)^6}{6!} \right|^2.$$

Here we proceed numerically. We find a maximal stability zone around $\tau = 1.49$ that is attained for $\zeta \approx 6.15$, as in the previous section. A non vanishing stability zone is obtained

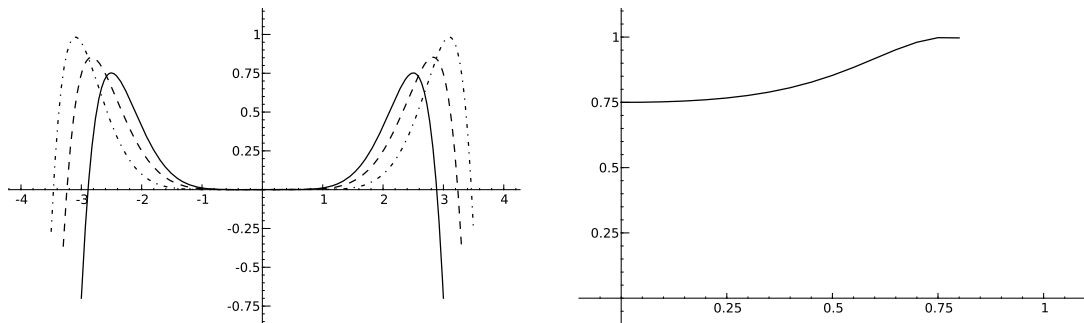


Figure 10: Order 4. Left. Plots of $D_{\zeta}(y)$ for $\zeta=0.1$ (solid), $\zeta=0.5$ (dash), $\zeta=5/6$ (dash-dot). Right. Maximum dissipation for different values of ζ going for 0 (minimal stability zone) to 5/6 (maximal stability zone).

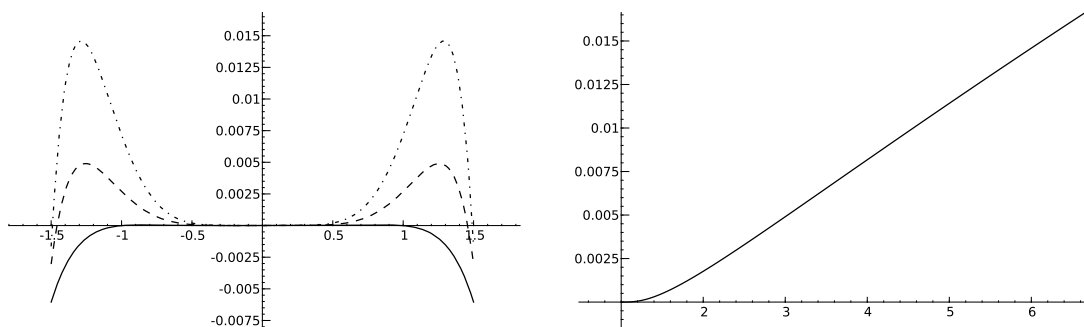


Figure 11: Order 5. Left. Plots of $D_{\zeta}(y)$ for $\zeta=1.2$ (solid), $\zeta=3$ (dash), $\zeta=6$ (dash-dot). Right. Maximum dissipation for different values of ζ going for 0 (minimal stability zone) to 6.15 (maximal stability zone).

for values of $\zeta > 1$ approximately. Here we are again in the case which is unstable for small values of ζ . Hence in order to have a small dissipation, one needs to take a small value of ζ but large enough so that the stability zone is not too small. Values of ζ close to 1.2 appear to be the most favorable. For example we have $\tau_{1.3} \approx 1.11$ and $\sigma(1.3) \approx 1.5 \times 10^{-4}$, and also $\tau_{1.2} \approx 1$ and $\sigma(1.2) \approx 5.26 \times 10^{-5}$.

Order 6. We have

$$D_{\zeta}(y) = 1 - T_{\zeta}(y) = 1 - \left| 1 + iy + \frac{(iy)^2}{2} + \frac{(iy)^3}{3!} + \frac{(iy)^4}{4!} + \frac{(iy)^5}{5!} + \frac{(iy)^6}{6!} + \zeta \frac{(iy)^7}{7!} \right|^2.$$

Numerically, we find a non vanishing stable zone around 0 for $0.88 \leq \zeta \leq 2.5$. For $\zeta = 0.9$, we have $\tau_{\zeta} \approx 0.89$ and $\sigma(\zeta) \approx 3.14 \times 10^{-7}$. For $\zeta = 1.05$, we have $\tau_{\zeta} \approx 1.98$ and $\sigma(\zeta) \approx 0.001$. For $\zeta = 2.5$, we have $\tau_{\zeta} \approx 2.75$ and $\sigma(\zeta) \approx 0.136$.

Summary. We notice a different behavior with respect to dissipation of the schemes that needed to be stabilized (orders 1,2,5,6) compared to the others (3 and 4). In the first case the curves for different values of ζ do not cross. So in this case the best choice is to take a value of ζ smaller than the one given the largest stability zone and to take a CFL condition

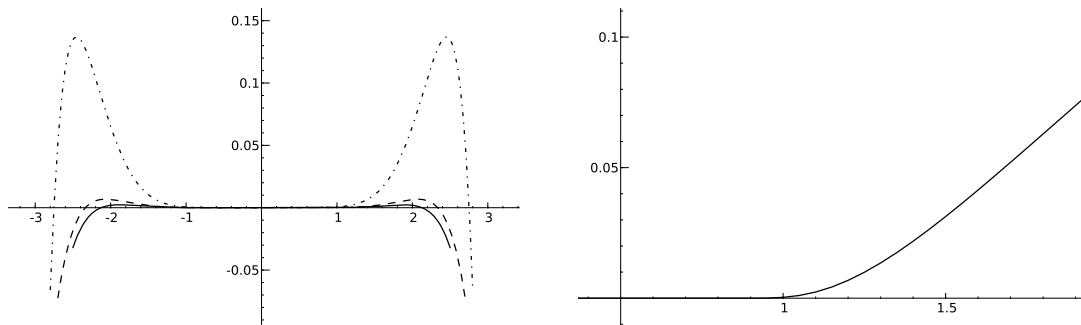


Figure 12: Order 6. Left. Plots of $D_\zeta(y)$ for $\zeta=1.1$ (solid), $\zeta=1.2$ (dash), $\zeta=2.5$ (dash-dot). Right. Maximum dissipation for different values of ζ going for 0.5 (minimal stability zone) to 2.8 (maximal stability zone).

corresponding to the stability condition for this ζ . In the other case, the curves cross, and the best option is to take the value of ζ giving the largest stability zone, but to take a CFL well below the stability condition in order to minimize dissipation. This effect was studied by Hu et al. [26].

We summarize in the following table, for different orders, values of ζ giving a fairly large stability zone for dissipation values always less than 1%.

Order	ζ	CFL	dissipation
1	1.11	0.59	0.0098
2	0.79	0.88	0.0011
2	0.77	0.62	0.00016
3	1	0.75	0.0022
3	1	0.5	0.00021
4	5/6	1	0.00053
4	5/6	0.5	5.5×10^{-5}
5	1.3	1.11	0.00015
5	1.2	1	5.26×10^{-5}
6	1.05	1.98	0.001
6	0.9	0.89	5×10^{-7}

4.2 High order symplectic time discretizations

Let us now introduce the symplectic time discretization schemes, starting again from the space discretized Maxwell equations (4.3)-(4.4) that we recall for convenience

$$\begin{cases} M_w \dot{E} - KB = 0, \\ M_v \dot{B} + K^T B = 0, \end{cases}$$

or in matrix form

$$\begin{aligned} \frac{d}{dt} \begin{pmatrix} E \\ B \end{pmatrix} &= \underbrace{\begin{pmatrix} 0 & M_w^{-1}K \\ -M_v^{-1}K^T & 0 \end{pmatrix}}_A \begin{pmatrix} E \\ B \end{pmatrix} \\ &= \underbrace{\begin{pmatrix} 0 & 0 \\ -M_v^{-1}K^T & 0 \end{pmatrix}}_T \begin{pmatrix} E \\ 0 \end{pmatrix} + \underbrace{\begin{pmatrix} 0 & M_w^{-1}K \\ 0 & 0 \end{pmatrix}}_V \begin{pmatrix} 0 \\ B \end{pmatrix}. \end{aligned}$$

After having introduced a uniform time discretization $t^n = n\Delta t$, for a time step Δt , the solution of the problem at time t^{n+1} can be expressed formally from the solution at time step t^n by

$$\begin{pmatrix} E^{n+1} \\ B^{n+1} \end{pmatrix} = \exp(\Delta t A) \begin{pmatrix} E^n \\ B^n \end{pmatrix} = \exp(\Delta t (T + V)) \begin{pmatrix} E^n \\ B^n \end{pmatrix}.$$

Assume now that we know a set of real numbers $\{(a_i, b_i), i = 1, \dots, p\}$, such that

$$\exp(\Delta t (T + V)) = \prod_{i=1}^p (\exp(a_i \Delta t T) \exp(b_i \Delta t V)) + \mathcal{O}(\Delta t^m),$$

then by definition

$$\prod_{i=1}^p (\exp(a_i \Delta t T) \exp(b_i \Delta t V)) \begin{pmatrix} E^n \\ B^n \end{pmatrix} \tag{4.7}$$

is an approximation of order m of $(E^{n+1} \ B^{n+1})^T$. Thus, it is possible to build symplectic time discretizations by finding $\{(a_i, b_i), i = 1, \dots, p\}$ using an identification of the terms of the development of the product $\prod_{i=1}^p (\exp(a_i \Delta t T) \exp(b_i \Delta t V))$ in powers of Δt with the terms of the development of $\exp(\Delta t (T + V))$.

The scheme defined by (4.7) can be obtained by the algorithm described in [32], that we adapt here to the system of equations we consider.

We initialize $B_{in} = B^n$ and $E_{in} = E^n$, where B^n and E^n denote the solution at time t^n and we iterate for i from 1 to p :

$$\begin{aligned} t_i &= t^n + \sum_{k=1}^{i-1} a_k \Delta t, \\ E_{out} &= E_{in} + b_i \Delta t M^{-1} (-K B_{in}), \\ B_{out} &= B_{in} + a_i \Delta t E_{out}, \\ E_{in} &\leftarrow E_{out}, \\ B_{in} &\leftarrow B_{out}, \end{aligned}$$

where the number of intermediate steps p , is equal to the order of the method for the first four orders and the coefficients $\{(a_i, b_i), i = 1, \dots, p\}$ are given in Table 1 for these orders.

For higher order methods, Yoshida proposes in [38] to compose methods of even order $(2m)$ with themselves to get a method of order $(2m + 2)$ in the following manner:

Table 1: Coefficients for symplectic time discretizations.

$p=1$	
$a_1=1$	$b_1=1$
$p=2$	
$a_1=\frac{1}{2}$	$b_1=0$
$a_2=\frac{1}{2}$	$b_2=1$
$p=3$	
$a_1=\frac{2}{3}$	$b_1=\frac{7}{24}$
$a_2=-\frac{2}{3}$	$b_2=\frac{3}{4}$
$a_3=1$	$b_3=-\frac{1}{24}$
$p=4$	
$a_1=\frac{2+2^{\frac{1}{3}}+2^{-\frac{1}{3}}}{6}$	$b_1=0$
$a_2=\frac{1-2^{\frac{1}{3}}-2^{-\frac{1}{3}}}{6}$	$b_2=\frac{1}{2-2^{\frac{1}{3}}}$
$a_3=\frac{1-2^{\frac{1}{3}}-2^{-\frac{1}{3}}}{6}$	$b_3=\frac{1}{1-2^{\frac{1}{3}}}$
$a_4=\frac{2+2^{\frac{1}{3}}+2^{-\frac{1}{3}}}{6}$	$b_4=\frac{1}{2-2^{\frac{1}{3}}}$

Denoting by S_{2m} the operator taking the solution from time t^n to time t^{n+1} , i.e.

$$\begin{pmatrix} E^{n+1} \\ B^{n+1} \end{pmatrix} = S_{2m}(\Delta t) \begin{pmatrix} E^n \\ B^n \end{pmatrix},$$

a method of order $(2m+2)$ is given by the composition

$$S_{2m+2}(\Delta t) = S_{2m}(\alpha\Delta t)S_{2m}(\beta\Delta t)S_{2m}(\alpha\Delta t),$$

with

$$\alpha = \frac{1}{2-2^{\frac{1}{2m+1}}} \quad \text{and} \quad \beta = -\frac{2^{\frac{1}{2m+1}}}{2-2^{\frac{1}{2m+1}}}.$$

Note that the fourth order discretization is the second order discretization composed with itself.

5 Efficiency of the time schemes

Let us now compare the efficiency of the different time schemes we just introduced by determining their stability conditions and evaluating their numerical dissipation and dispersion. We want to find out in particular if the numerical order of the schemes corresponds to the theoretical order and if the mass lumping does not lead to a decrease in order.

5.1 Rectangular edge finite elements on structured meshes

We consider here the edge finite elements on quads defined in Subsection 2.2 and their lumped version defined in Section 3.

Let us first determine the stability limit by propagating a plane wave across a diagonal of the domain $\Omega = [0,1] \times [0,1]$ so that we do not favor one of the directions. Indeed, we solve the following problem

$$\begin{cases} \frac{\partial \mathbf{E}}{\partial t} - \nabla \times B = 0, \\ \frac{\partial B}{\partial t} + \nabla \times \mathbf{E} = 0, \\ \mathbf{E}(x,y,0) = \begin{pmatrix} \frac{\alpha w}{2k} \sin(k(x-y)) \\ \frac{\alpha w}{2k} \sin(k(x-y)) \end{pmatrix}, \\ B(x,y,0) = \alpha \sin(k(x-y)), \end{cases} \quad (5.1)$$

with $w = \sqrt{2k}$, the solution of which is given by

$$\begin{aligned} \mathbf{E}(x,y,t) &= \begin{pmatrix} \frac{\alpha w}{2k} \sin(k(x-y) - wt) \\ \frac{\alpha w}{2k} \sin(k(x-y) - wt) \end{pmatrix}, \\ B(x,y,t) &= \alpha \sin(k(x-y) - wt). \end{aligned}$$

We call optimal CFL numbers the largest CFL numbers that allow us to propagate stably the wave over a hundred periods. These optimal CFL numbers are given for each time discretization in Table 2 for the discretization by standard edge elements and in Table 3 for the lumped edge elements. Notice that for lumped elements, optimal CFL numbers are slightly higher.

The convergence orders are determined on the same test case after one (theoretical) propagation period and listed in Table 4 for standard edge elements space discretization and in Table 5 for the lumped edge elements. We only give here the convergence orders

Table 2: Optimal CFL number for edge element space discretization and stabilized Taylor expansion and symplectic time discretizations.

Theoretical order of the discretization	1	2	3	4	5
stabilized Taylor expansion	0.20	0.18	0.093	0.10	0.038
symplectic	0.40	0.18	0.13	0.057	0.041

Table 3: Optimal CFL number for lumped edge element space discretization and stabilized Taylor expansion and symplectic time discretizations.

Theoretical order of the discretization	1	2	3	4	5
stabilized Taylor expansion	0.35	0.28	0.14	0.14	0.053
symplectic	0.70	0.28	0.20	0.082	0.056

Table 4: Numerical convergence order for standard edge elements.

Theoretical order of the discretization	1	2	3	4	5
stabilized Taylor expansion	0.94	1.97	2.99	3.99	4.99
symplectic	1.01	2.00	2.99	3.99	4.99

Table 5: Numerical convergence order for lumped edge elements.

Theoretical order of the discretization	1	2	3	4	5
stabilized Taylor expansion	0.94	1.99	2.99	3.99	4.99
symplectic	1.00	2.00	2.99	3.99	4.99

for the magnetic field in L^2 -norm and we verified that those for the electric field are equivalent. We can observe that these convergence orders are in agreement with the theory and that the mass lumping does not decrease this order.

Let us now come to the cost versus precision rate for our different schemes by finding out the total number of degrees of freedom for the electric field and the magnetic field (denoted respectively by #DOF_E et #DOF_B) and the computation time needed to reach an error (on the magnetic field in L^2 -norm) less than a given threshold, after 10 (theoretical) propagation periods. The results appear in Tables 6 to 9 for error thresholds from 1.36×10^{-3} to 1.25×10^{-9} . In these tables and accompanying remarks we denote by *Taylor* our stabilized Taylor expansion time scheme and by *symplectic* the symplectic time discretization of corresponding order. In order to pinpoint the advantage of taking a time step lowering the dissipation, we tested different values of ζ for orders 1 and 2 and noticed that the dissipation optimized time step is preferable. In our tests dissipation was

Table 6: Computation cost (in time and number of DOFs) to reach an error (on the magnetic field in $L^2(\Omega)$ norm) less than 1.36×10^{-3} .

error $< 1.36 \times 10^{-3}$					
Space Disc.	Time Disc.	CFL number	error_E error_B	#DOF_E #DOF_B	CPU time
Standard order 1	Taylor $\zeta = 2., \Delta_t opt.$	0.20	9.58×10^{-4} 1.36×10^{-3}	26912 13456	375.s
Standard order 1	Taylor $\zeta = 1.1642, \Delta_t opt.$	0.16	9.49×10^{-4} 1.34×10^{-3}	968 484	1.s
Standard order 1	symplectic	0.40	8.84×10^{-4} 1.28×10^{-3}	800 400	<1.s
Lumped order 1	Taylor $\zeta = 2., \Delta_t opt.$	0.35	9.68×10^{-4} 1.36×10^{-3}	81608 40804	50.s
Lumped order 1	Taylor $\zeta = 1.1642, \Delta_t opt.$	0.27	9.49×10^{-4} 1.34×10^{-3}	1352 676	<1.s
Lumped order 1	symplectic	0.70	8.16×10^{-4} 1.32×10^{-3}	162 81	<1.s

Table 7: Computation cost (in time and number of DOFs) to reach an error (on the magnetic field in $L^2(\Omega)$ norm) less than 1.01×10^{-5} .

error $< 1.01 \times 10^{-5}$					
Space Disc.	Time Disc.	CFL number	error_E error_B	#DOF_E #DOF_B	CPU time
Standard order 2	Taylor $\xi = 1.5, \Delta_t opt.$	0.18	7.06×10^{-6} 1.01×10^{-5}	38088 19044	621.s
Standard order 2	Taylor $\xi = 0.8663, \Delta_t opt.$	0.13	5.96×10^{-6} 9.83×10^{-6}	8192 4096	39.s
Standard order 2	symplectic	0.18	6.92×10^{-6} 1.00×10^{-5}	20000 10000	123.s
Lumped order 2	Taylor $\xi = 1.5, \Delta_t opt.$	0.28	7.13×10^{-6} 1.01×10^{-5}	38088 19044	98.s
Lumped order 2	Taylor $\xi = 0.8663, \Delta_t opt.$	0.21	1.05×10^{-5} 9.54×10^{-6}	16200 8100	7.s
Lumped order 2	symplectic	0.28	7.06×10^{-6} 1.00×10^{-5}	46208 23104	26.s

Table 8: Computation cost (in time and number of DOFs) to reach an error (on the magnetic field in $L^2(\Omega)$ norm) less than 5.32×10^{-8} .

error $< 5.32 \times 10^{-8}$					
Space Disc.	Time Disc.	CFL number	error_E error_B	#DOF_E #DOF_B	CPU time
Standard order 3	Taylor optimal Δ_t	0.093	3.35×10^{-8} 5.76×10^{-8}	45000 22500	1098.s
Standard order 3	symplectic	0.13	2.64×10^{-8} 5.31×10^{-8}	31752 15876	432.s
Lumped order 3	Taylor optimal Δ_t	0.14	3.74×10^{-8} 5.37×10^{-8}	88200 44100	179.s
Lumped order 3	Taylor Δ_t constrained	0.059	2.72×10^{-8} 5.21×10^{-8}	33282 16641	74.s
Lumped order 3	symplectic	0.20	2.64×10^{-8} 5.31×10^{-8}	31752 15876	26.s

very low in any case for the order 5 scheme.

Let us notice the superiority in terms of number of degrees of freedom for the high order schemes: For example only 4900 degrees of freedom are necessary for the order 5 scheme to reach an error less than 1.25×10^{-9} on the magnetic field whereas 19600 are necessary for the order 4 scheme. However this does not necessarily lead to a smaller computation time. The lumped space discretization combined with the Taylor expansion of order 4 only needs 134 seconds to reach an error less than 1.25×10^{-9} whereas the standard edge element space discretization of order 5 combined with the stabilized Taylor expansion of same order takes 195 seconds. We notice the gain of using the lumped edge finite elements versus the standard elements for all orders.

Table 9: Computation cost (in time and number of DOFs) to reach an error (on the magnetic field in $L^2(\Omega)$ norm) less than 1.25×10^{-9} .

error $< 1.25 \times 10^{-9}$					
Space disc.	Time disc.	CFL Number	error_E error_B	#DOF_E #DOF_B	CPU time
Standard order 4	Taylor	0.10	6.72×10^{-10} 1.15×10^{-9}	41472 20736	833.s
Standard order 4	symplectic	0.057	6.92×10^{-10} 1.22×10^{-9}	39200 19600	1303.s
Lumped order 4	Taylor	0.14	7.89×10^{-10} 1.15×10^{-9}	61952 30976	134.s
Lumped order 4	symplectic	0.082	8.13×10^{-10} 1.18×10^{-9}	61952 30976	229.s
Standard order 5	Taylor	0.038	4.60×10^{-10} 9.07×10^{-10}	9800 4900	195.s
Standard order 5	symplectic	0.041	4.55×10^{-10} 9.07×10^{-10}	9800 4900	360.s
Lumped order 5	Taylor	0.053	4.60×10^{-10} 9.17×10^{-10}	9800 4900	24.s
Lumped order 5	symplectic	0.056	4.55×10^{-10} 9.07×10^{-10}	9800 4900	43.s

Notice also that the comparison of the time discretizations depends on the order of the scheme: For orders 1, 2 and 3 symplectic time discretizations are at a large advantage in computation cost whereas they become more expensive for orders 4 and 5. For the plane wave propagation the order 4 and 5 Taylor expansion schemes have dissipation and dispersion errors close to machine accuracy which makes them more efficient than the more involved symplectic schemes in this case.

5.2 Triangular finite elements

We consider in this section the triangular edge elements introduced in Subsection 2.2. For the triangular edge elements we shall merely determine the highest CFL numbers giving numerical stability and verify the convergence orders, the conclusion on the cost vs. precision tests being similar to the quadrilateral finite elements. We now propagate a plane wave along the horizontal axis, *i.e.* we solve the problem

$$\begin{cases} \frac{\partial \mathbf{E}}{\partial t} - \nabla \times \mathbf{B} = 0, \\ \frac{\partial \mathbf{B}}{\partial t} + \nabla \times \mathbf{E} = 0, \\ \mathbf{E}(x, y, 0) = \begin{pmatrix} 0 \\ \alpha \sin(kx) \end{pmatrix}, \\ \mathbf{B}(x, y, 0) = \alpha \sin(kx), \end{cases} \quad (5.2)$$

Table 10: Optimal CFL numbers of stabilized Taylor expansion and symplectic time discretization.

Theoretical order of discretization	1	2	3	4	5
Stabilized Taylor expansion	0.23	0.24	0.13	0.14	0.056
Symplectic	0.47	0.24	0.19	0.082	0.060

Table 11: Numerical convergence order.

Theoretical order of discretization	1	2	3	4	5
Stabilized Taylor expansion	0.93	1.99	2.99	3.99	5.34
Symplectic	1.00	2.00	2.99	4.05	5.02

the solution of which being given by

$$\mathbf{E}(x,y,t) = \begin{pmatrix} 0 \\ \alpha \sin(k(x-t)) \end{pmatrix},$$

$$B(x,y,t) = \alpha \sin(k(x-t)),$$

where we adapt k to the computation domain in order to remain coherent with the periodic boundary conditions. On the computational domain $[-5,5] \times [-2.5,2.5]$ with $k=2\pi$, we have determined the stability limit of our schemes and listed the results in Table 10 for stabilized Taylor expansion and symplectic time discretizations.

The convergence orders are determined for the optimal CFL numbers by propagating a plane wave of wave length 1 along the horizontal axis of the domain $[0,1] \times [0,1]$ for one period. These orders are listed in Table 11.

5.3 Conformal coupling of triangular and quadrilateral edge elements

Let us now test the coupling between the lumped edge elements on a uniform quadrilateral mesh and the triangular edge elements. To this aim, we have propagated an initial impulsion derived from a Gaussian on a circular domain with an absorbing Silver-Müller boundary condition, first on a hybrid mesh and then on a fully triangle mesh. The meshes are represented in Fig. 13 and have an almost identical number of degrees of freedom for a given order. These numbers are given in Table 12.

Table 12: Number of degrees of freedom for each order on hybrid mesh and triangle mesh.

Theoretical order of discretization	1	2	3	4	5
#DOF electric field :					
hybrid mesh	1795	6450	13965	24340	37575
triangle mesh	2015	6650	13905	23780	36275
#DOF magnetic field :					
hybrid mesh	1030	3490	7380	12700	19450
triangle mesh	1310	3930	7860	13100	19650

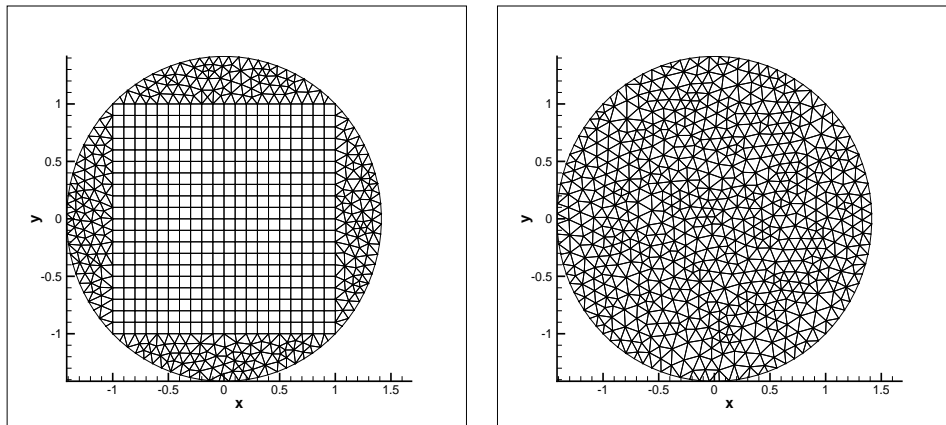


Figure 13: Hybrid mesh and triangle mesh of domain.

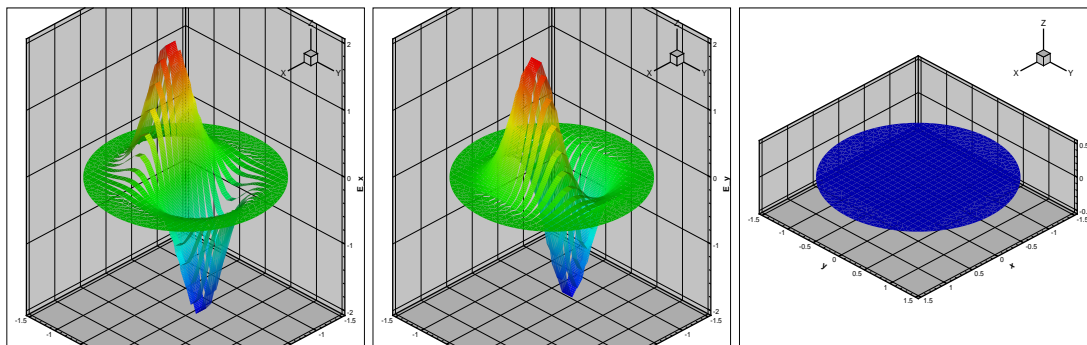


Figure 14: Initial impulse with lowest order edge elements on hybrid mesh.

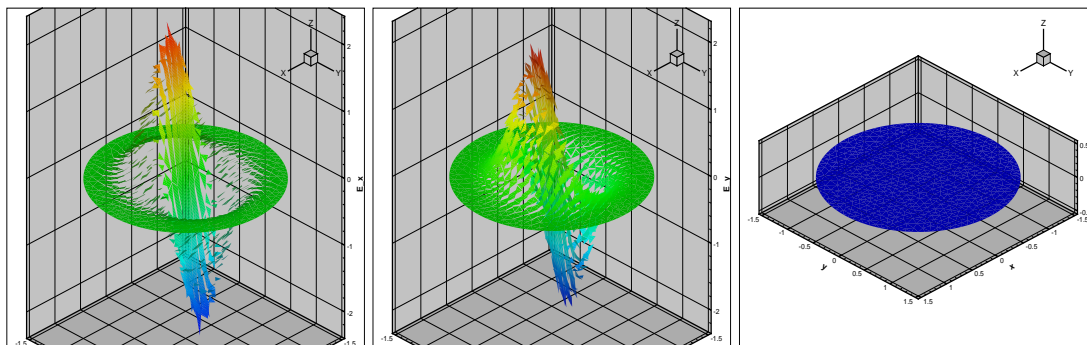
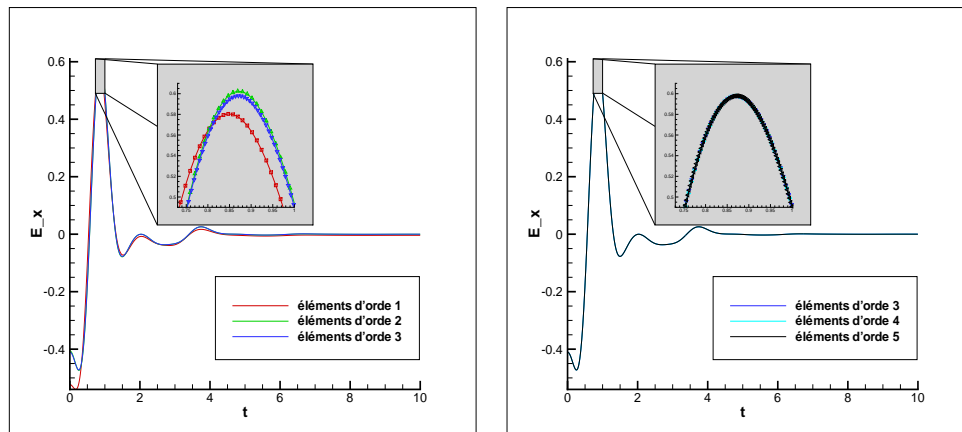
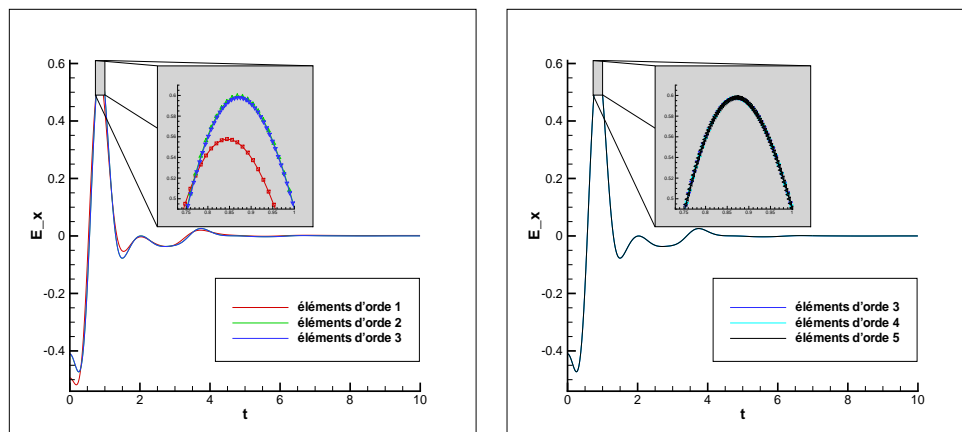


Figure 15: Initial impulse with lowest order edge elements on unstructured triangle mesh.

Figs. 14 and 15 represent the projections of the initial impulse on the discretization spaces associated to the schemes of lowest order for the hybrid mesh and the triangle mesh.

Figure 16: First component of electric field at point $(0.5,0.5)$ on hybrid mesh.Figure 17: First component of electric field at point $(0.5,0.5)$ for triangle mesh.

We first consider the time evolution of the first component of the electric field at point $(0.5,0.5)$, this point is in the uniform part of the mesh for the hybrid mesh. Fig. 16 displays the results for the hybrid mesh, and Fig. 17 for the triangle mesh.

Notice that the behavior of the discretization on both meshes are very similar. For orders 1, 2 and 3 the solutions are different but with identical profiles and for higher orders the solutions become identical. Remember that one of our objectives in using hybrid meshes was the existence of a mass lumped element on the regular part of the mesh. Table 13 gives the computation times on both meshes for each order. We notice a decrease of the computation time for the coupled finite elements. Note that this gain could still be improved by adjusting more precisely the region where quadrilateral cells are used to the shape of the computational domain. This will be useful in cases where the computational domain cannot be meshed only using quads.

Table 13: Compared computation time for hybrid and triangle meshes.

Theoretical order of discretization	1	2	3	4	5
CPU time on hybrid mesh	<1.s	5.s	32.s	88.s	653.s
CPU on triangle mesh	<1.s	7.s	43.s	116.s	827.s

6 Conclusion

We have investigated different schemes for solving the Maxwell equations in the time domain on complex geometries. We have introduced an edge finite element method on hybrid triangle and quad meshes which has proved efficient. Indeed, on the structured quad mesh we can use mass lumped elements and thus reduce the time of the computation for obtaining the same results as those on a complete unstructured mesh. We have also introduced a high-order time discretization scheme based on a Taylor expansion that can be stabilized if necessary. We have shown that using symplectic schemes is interesting for low order but becomes more expensive for order 4 and more. Our time schemes of order 4 and more are thus very competitive as the dissipation and dispersion errors are close to machine accuracy.

Acknowledgments

This work was partially supported by the Agence Nationale de la Recherche, ANR-06-CIS6-0013.

References

- [1] F. Assous, P. Degond, E. Heintze, P.-A. Raviart, J. Segré, On a finite-element method for solving the three-dimensional Maxwell equations, *J. Comput. Phys.* 109 (1993), no. 2, 222-237.
- [2] N. Canouet, L. Fezoui, S. Piperno, Discontinuous Galerkin time-domain solution of Maxwell's equations on locally-refined nonconforming Cartesian grids, *COMPEL* 24 (2005), no. 4, 1381-1401.
- [3] P. Castillo, R. Rieben, D. White, FEMSTER: An object oriented class library of high-order discrete differential forms, *ACM Trans. Math. Softw.* 31 (2005), no. 4.
- [4] P. J. Channell, C. Scovel, Symplectic integration of Hamiltonian systems, *Nonlinearity* 3 (1990), 231-259.
- [5] M. J. S. Chin-Joe-Kong, W. A. Mulder, M. Van Veldhuizen, Higher-order triangular and tetrahedral finite elements with mass lumping for solving the wave equation, *J. Engrg. Math.* 35 (1999), no 4, 405-426.
- [6] G. Cohen, *Higher-Order Numerical Methods for Transient Wave equation*, Springer-Verlag, 2001.
- [7] G. Cohen, M. Duruflé, Non spurious spectral-like element methods for Maxwell's equations, *J. Comput. Math.* 25 (2007), no. 3, 282-304.

- [8] G. Cohen, P. Monk, Mur-Nédélec finite element schemes for Maxwell's equations, *Comput. Methods Appl. Mech. Engrg.* 169 (1999), no. 3-4, 197-217.
- [9] G. Cohen, P. Monk, Gauss point mass lumping schemes for Maxwell's equations, *Numer. Meth. Part. D. E. J.* 14 (1998), No. 1, 63-88.
- [10] M. A. Dablain, The application of high order differencing for the scalar wave equation, *Geophysics* 51 (1986), No. 1, 54-66.
- [11] J.C. Gilbert, P. Joly, Higher order time stepping for second order hyperbolic problems and optimal CFL conditions, *Partial differential equations*, 67-93, *Comput. Methods Appl. Sci.* 16, Springer, Dordrecht, 2008.
- [12] M. Dumbser, C.-D. Munz, Arbitrary High Order Discontinuous Galerkin Schemes, *Numerical Methods for Hyperbolic and Kinetic Problems*, eds. S. Cordier, T. Goudon, M. Gutnic, E. Sonnendrücker, IRMA series in Mathematics and Theoretical Physics, European Mathematical Society, 2005.
- [13] M. Dumbser, C.-D. Munz, ADER discontinuous Galerkin schemes for aeroacoustics, *C. R. Mécanique* 333-9 (2005), 683-687.
- [14] A. Elmkies, P. Joly, Edge finite elements and mass lumping for Maxwell's equations: The 2D case, *C. R. Acad. Sci. Paris* 324 (1997), Série I, 1287-1293.
- [15] A. Elmkies, P. Joly, Edge finite elements and mass lumping for Maxwell's equations: The 3D case, *C. R. Acad. Sci. Paris* 325 (1997), Série I, 1217-1222.
- [16] L. Fezoui, S. Lanteri, S. Lohrengel, S. Piperno, Convergence and stability of a discontinuous Galerkin time-domain method for the 3D heterogeneous Maxwell equations on unstructured meshes, *Math. Model. Numer. Anal.* 39 (2005), no. 6, 1149-1176.
- [17] A. Fisher, R. N. Rieben, G. Rodrigue, D. A. White, A generalized mass lumping technique for vector finite-element solutions of the time-dependent Maxwell equations, *IEEE T. Antenn. Propag.* 53 (2005), no. 9, 2900-2910.
- [18] D. Gaitonde, J. S. Shang, Optimized compact-difference-based finite-volume schemes for linear wave phenomena, *J. Comput. Phys.* 138 (1997), no. 2, 617-643.
- [19] S. Gottlieb, L.-A. J. Gottlieb, Strong stability preserving properties of Runge-Kutta time discretization methods for linear constant coefficient operators, *J. Sci. Comput.* 18 (2003), no. 1, 83-109.
- [20] S. Gottlieb, C.-W. Shu, E. Tadmor, Strong stability-preserving high-order time discretization methods, *SIAM Rev.* 43 (2001), no. 1, 89-112.
- [21] A. Harten, B. Engquist, S. Osher, S. Chakravarthy, Uniformly high order essentially non-oscillatory schemes, III, *J. Comput. Phys.* 71 (1987), 231-303.
- [22] J. S. Hesthaven, High-Order Accurate Methods in Time-Domain Computational Electromagnetics. A Review, *Adv. Imag. Electron Phys.* 127 (2003), 59-123.
- [23] J. S. Hesthaven and T. Warburton, Nodal high-order methods on unstructured grids, I. Time-domain solution of Maxwell's equations, *J. Comput. Phys.* 181 (2002), 186-221.
- [24] J. S. Hesthaven and T. Warburton, *Nodal Discontinuous Galerkin Methods: Algorithms, Analysis, and Applications*, Springer (2007).
- [25] R. Hiptmair, Finite elements in computational electromagnetism, *Acta Numerica* (2002), 237-339.
- [26] F. Q. Hu, M. Y. Hussaini, J. L. Manthey, Low-dissipation and low-dispersion Runge-Kutta schemes for computational acoustics, *J. Comput. Phys.* 124 (1996), 177-191.
- [27] P. Lacoste, Mass-lumping for first-order Raviart-Thomas-Nédélec mixed finite elements, *C. R. Math. Acad. Sci. Paris* 339 (2004), no. 10, 727-732.
- [28] P. Monk, *Finite Element Methods for Maxwell's Equations*, Oxford University Press, 2003.

- [29] J.-C. Nédélec, Mixed finite elements in \mathbb{R}^3 , *Numer. Math.* 35 (1980), 315-341.
- [30] S. Pernet, X. Ferrieres, G. Cohen, High spatial order finite element method to solve Maxwell's equations in time domain, *IEEE T. Antenn. Propag.* 53 (2005), no. 9, 2889-2899.
- [31] S. Piperno, Symplectic local time-stepping in non-dissipative DGTD methods applied to wave propagation problems, *Math. Model. Numer. Anal.* 40 (2006), no. 5, 815-841.
- [32] R. Rieben, D. White, and G. Rodrigue, High Order Symplectic Integration Methods for Finite Element Solutions to Time Dependent Maxwell Equations, *IEEE T. Antenn. Propag.* 52 (2004), no. 8, 2190-2195.
- [33] G. Rodrigue, D. White, A vector finite element time-domain method for solving Maxwell's equations on unstructured hexaedral grids, *SIAM J. Sci. Comput.* 23 (2001) no. 3, 683-706.
- [34] G. R. Shubin, J. B. Bell, A modified equation approach to constructing fourth-order methods for acoustic wave propagation, *SIAM J. Sci. Statist. Comput.* 8 (1987), no. 2, 135-151.
- [35] D. Sármany, M.A. Botchev, J. J. W. van der Vegt, Dispersion and dissipation error in high-order Runge-Kutta discontinuous Galerkin discretizations of the Maxwell equations, *J. Sci. Comput.* 33 (2007), no. 1, 47-74.
- [36] T. Warburton, An explicit construction for interpolation nodes on the simplex, *J. Engrg. Math.* 56 (2006), no. 3, 247-262.
- [37] K. S. Yee, Numerical solution of initial boundary value problems involving Maxwell's equations in isotropic media, *IEEE T. Antenn. Propag.* 14 (1966).
- [38] H. Yoshida, Construction of higher order symplectic integrators, *Phys. Lett. A* 150 (1990), no. 5-7, 262-268.